THE JOURNAL OF PHYSICAL CHEMISTRY B

Article

pubs.acs.org/JPCB

Cell Penetrating Peptide Adsorption on Magnetite and Silica Surfaces: A Computational Investigation

Gianvito Grasso,[†,‡] Marco A. Deriu,[†] Maria Prat,[‡] Lia Rimondini,[‡] Enrica Vernè,[§] Antonia Follenzi,*[,‡] and Andrea Danani*[,†]

[†]Department of Innovative Technologies, University for Applied Sciences of Southern Switzerland (SUPSI), Centro Galleria 2, Manno CH-6928, Switzerland

[‡]Department of Health Sciences, Università degli Studi del Piemonte Orientale "A. Avogadro", via Paolo Solaroli 17, Novara IT-28100, Italy

[§]Department of Applied Science and Technology, Politecnico di Torino, Corso Duca degli Abruzzi 24, Torino IT-10129, Italy

Supporting Information

ABSTRACT: Magnetic nanoparticles (MNPs) represent one of the most promising materials as they can act as a versatile platform in the field of bionanotechnology for enhanced imaging, diagnosis, and treatment of various diseases. Silica is the most common compound for preparing coated iron oxide NPs since it improves colloidal stability and the binding affinity for various organic molecules. Biomolecules such as cell penetrating peptides (CPPs) might be employed to decorate MNPs, combining their promising physicochemical properties with a cell penetrating ability. In this work, a computational investigation on adsorption of *Antennapedia* homeodomain-derived penetrating peptide (pAntp) on silica and magnetite (MAG) surfaces is presented. By employing umbrella sampling molecular dynamics, we provided a quantitative estimation of the pAntp−surface adsorption free energy to highlight the influence of surface hydroxylation state on the adsorption mechanism. The interaction between peptide and surface has shown to be mainly driven by electrostatics. In case of MAG surface, also an important contribution of van der Waals (VdW) attraction was observed. Our data suggest that a competitive mechanism between MNPs and cell membrane might partially inhibit the CPP to carry out its membrane penetrating function.

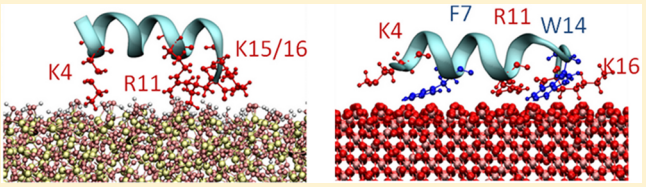

INTRODUCTION

The discovery of cell-penetrating peptides (CPPs) represents an important breakthrough for the delivery of large cargo molecules or nanoparticles for several clinical applications. A main feature of CPPs is the ability to penetrate the cell membrane at low micromolar concentrations *in vivo* and *in vitro*, without binding any chiral receptor and without causing significant membrane damage.[1]

TAT peptide[2,3] and Drosophila *Antennapedia* homeodomain-derived penetrating peptide (pAntp)[4,5] are the most extensively studied CPPs. In particular, the pAntp is a 16-residue long cationic peptide derived from the third helix of the homeodomain of the *Drosopyila* transcription factor *Antennapedia*. This amphipatic CPP is positively charged at neutral pH (since it contains four lysine and three arginine residues). Interestingly, the pAntp is able to cross the biological membrane and to penetrate a hydrophobic environment upon interaction with negatively charged molecules like phosphatic acid (PA) or phosphatidylserine (PS).[6] However, mechanisms by which pAntp comes into the cells have not been completely understood. Proposed mechanisms[7,8] of pAntp cellular uptake hypothesize direct crossing of the peptide through the membrane at low peptide concentrations (1 μM) and an endocytotic pathway at high concentrations (10 μM). A number of studies have suggested that pAntp amphiphilicity may not be enough to drive the membrane penetration, indicating instead tryptophan as key player.[9] Replacement of tryptophan by phenylalanine resulted in a loss of penetration activity when interacting with membranes and bicelles. Moreover, a recent computational work has characterized the mechanism by which pAntp binds to DPPC bilayers, proposing arginine, lysine, and tryptophan as driving the penetration.[10] This extraordinary ability of CPPs to penetrate the cell membrane has brought to designate them as perfect functionalization molecules for drug delivery systems.

For example, pAntp might be employed to decorate magnetic nanoparticles (MNPs), thus combining their fascinating physicochemical properties with a cell penetrating ability to design novel effective therapeutic strategies as well as innovative biotechnology methodologies. Size, biocompatibility, and excellent magnetic properties have made MAG and silica-coated MAG the object of a remarkable amount of research in the past decade, and numerous biomedical applications have been reported.[11−13] Recently, MNPs combined with magnetic

Received: December 22, 2014
Revised: June 3, 2015
Published: June 4, 2015

DOI: 10.1021/jp512782e
J. Phys. Chem. B 2015, 119, 8239−8246

fields were used to enable cell positioning under nonpermissive conditions, local gene therapy, and/or optimization of MNP-assisted lentiviral gene transfer.[14−16]

Functionalization strategies comprise, among others, grafting with organic molecules, including small biomolecules such as CPPs and/or coating with an inorganic layer (e.g., silica).[17−20]

Design and properties prediction of functionalization strategies may be addressed by computational molecular modeling. In this context, Kubiak-Ossowska and co-workers have recently employed computational modeling to investigate the adsorption of TAT peptides onto three silica surface models.[21] This work has suggested that TAT−silica adsorption mechanism is driven by electrostatic and hydrophobic interactions mainly involving arginine residues and the nanoparticle surface.

Here, we focus our attention on the pAntp and its adsorption on MAG and silica surfaces. A computational study aimed at understanding the noncovalent interactions between pAntp and MAG/silica surfaces is reported. Estimating the affinity of different surfaces for the same peptide is one example where the calculation of the free energy profile plays a relevant role. Most free energy calculations are generally formulated by estimating the relative free energy differences, ΔG, between two equilibrium states. The free energy calculation could require to overcome high energy barriers ($E_{barrier} \gg kT$), rarely sampled by equilibrium MD simulations. Thus, the conformational ensemble provided by classical MD simulations might not be adequate. In this connection, enhanced sampling methods represent a powerful tool to improve the sampling efficiency of classical MD, including those that artificially add external driving forces to guide the protein from one structure to another. In this work, binding free energy has been evaluated by means of umbrella sampling molecular dynamics. Following this approach we have investigated the effect of different hydroxylation states on the pAntp−surface adsorption properties.

With respect to previous literature and in particular to the interesting investigation of Kubiak-Ossowska and co-workers,[21] we highlight some elements of difference in our work: (1) we focused our investigation on the pAnt CPP, (2) we have investigated the CPP adsorption onto both silica and magnetite, and (3) we have employed both classic MD and umbrella sampling to investigate the CPP adsorption over a specific surface.

Our data are in agreement with previous works, highlighting that the pAntp−surface adsorption, like the TAT−surface interaction,[21] is mainly driven by electrostatics and involves arginine, lysine, and tryptophan. Thus, a competitive mechanism between MNPs and cell membrane, both interacting with the same sites of pAntp, might partially inhibit the CPP to carry out its penetrating function.

MATERIALS AND METHODS

Preparation of the Amorphous Silica Surface. The atomic structure of the amorphous silica has been modeled by means of the Inorganic Builder Plugin of the Visual Molecular Dynamics tool.[22] The size of the silica cubic unit cell was 7.16 Å and contained 24 atoms, 8 silicon and 16 oxygen atoms, resulting in an oxygen/silicon ratio of 2:1. For the surface model, a slab of amorphous silica with dimensions 40 Å × 40 Å × 20 Å was generated. Two variants of the surface were created: silica surface with siloxide (SiO−) groups only on the top (named SIO_2); fully hydroxylated silica surface decorated by silanol (Si−OH) groups (named $hSiO_2$).

The silanol density and type, determining the hydrophilicity of the surface, are related. Three different types of silanol can be identified: single silanol, geminal (two hydroxyl groups per silicon), and vicinal or bridged OH groups. Each type of silanol shows different hydrophilicity, hydrogen-bonding affinity, and adsorption energy. In particular, for a hydroxyl site density greater than 3 per nm^2, almost all of the silanol groups on the surface are isolated,[23] in close agreement with our $hSiO_2$. The $hSiO_2$ model was obtained by saturating the dangling silicon and oxygen atoms with hydroxyl groups and hydrogen, respectively, following the computational procedure carried out in a recent work.[24] The obtained silanol density in the $hSiO_2$ surface model is about 5 per nm^2 according to Zhuravlev's model.[23]

The clay force field[25] (hydroxyl bonds and silanol angles) have been employed for the surface topology. The clay force field, parametrized for biochemical simulations, provides a high degree of flexibility in term silica decoration with organic molecules.[24] Moreover, it has proven to be very successful in describing the water−silica interaction in comparison to scattering experiments and *ab initio* simulations.[26,27] Partial charges optimization was performed by using GULP[28] (Rappe and Goddard's charge equilibration method[29]). During the MD simulations, the bulk of the plates was restrained, and only the silanol groups and their neighboring bulk oxygen atoms were allowed to move.

Preparation of the Magnetite Surface. The MAG atomic coordinates were obtained by Crystallography Open Database (COD ID: 1011084). The unit cell has a size of 8.39 Å and contains 28 atoms, 12 iron and 16 oxygen atoms, resulting in an oxygen/iron ratio of 4:3. For the MAG surface model, a slab of 40 Å × 40 Å × 20 Å was generated. Two variants of the surface were created: MAG surface with FeO groups only on the top (named MAG); fully hydroxylated MAG surface decorated by Fe−OH) groups (named hMAG). The hMAG model was obtained following the same procedure carried out for the amorphous silica preparation. More in depth, the dangling iron and oxygen atoms were saturated with hydroxyl groups and hydrogens, respectively. Clay force field[25] (hydroxyl bonds and Fe−O−H angle) have been employed for MAG topology. Partial charges optimization was performed by using GULP[28] (Rappe and Goddard's charge equilibration method[29]).

Preparation of the PAntp Model. The NMR model of the pAntp (sequence RQIKIWFQNRRMKWKK) was taken from the Protain Data Bank (PDB ID: 1OMQ[30]) . The CHARMM22/CMAP[31,32] force field was employed to define the pAntp topology, since that it has been demonstrated that the CLAYFF and CHARMM force fields are compatible and can be used together.[27,33−35]

Molecular Dynamics. We set up four different molecular systems: (a) MAG−pAntp, (b) hMAG−pAntp, (c) SIO_2−pAntp, and (d) $hSIO_2$−pAntp. The pAntp is placed at 2 nm from the surface center of mass (COM). Each molecular system, initially placed in a cubic box of 6 nm × 6 nm × 6 nm and explicitly solvated, consisted of about 40 000 interacting particles.

The above-mentioned systems were first minimized by steepest descent energy minimization algorithm followed by a preliminary position restrain MD of about 100 ps in isothermal−isobaric ensemble. A steered molecular dynamics

DOI: 10.1021/jp512782e
J. Phys. Chem. B 2015, 119, 8239−8246

(SMD) simulation applied to the peptide CoM was carried out on each system to obtain a number of initial configurations for the umbrella sampling (US) along the reaction coordinate, i.e., the pAntp/surface-COM distance (Figure 1). In detail, the pAntp was moved toward the surface by imposing a "constant velocity" pull harmonic potential during a MD of 250 ps in a NVT ensemble. Snapshots were recorded every 2 ps, resulting in a reasonable distribution of initial US configurations. In this way, enough configurations were captured, thus obtaining a regular spacing of 0.15 nm along the reaction coordinate.

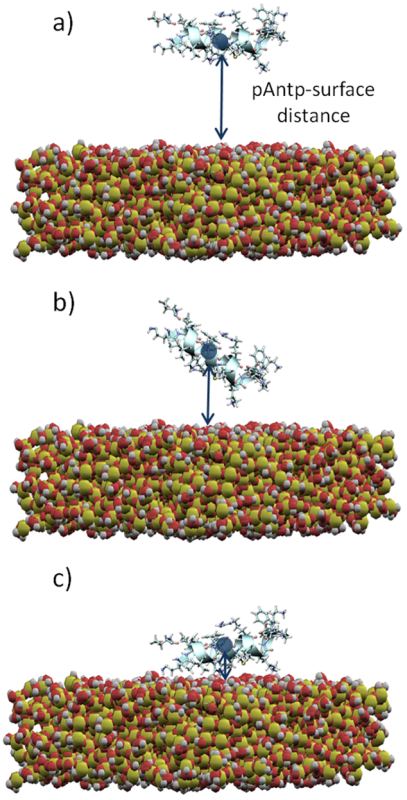

Figure 1. Steered MD configurations in the case of pAntp-hSIO system. The peptide CoM−surface slab initial distance was set up to 2 nm (a). A steered molecular dynamics simulation was carried out in order to obtain a number of initial configurations for the umbrella sampling along the reaction coordinate (e.g., b and c), i.e., the pAntp−COM/surface distance.

On each configuration a preliminary position restrained MD in the NVT ensemble at 300 K was carried out for 50 ps (restraints applied to the peptide backbone). Each system was then simulated (2 fs time step) for 30 ns in the NVT ensemble by applying a umbrella biasing potential with force constant of 1000 kJ mol^{-1} nm^2 to constrain the distance between pAntp and surface center of mass. The pAntp−surface energy profile was estimated by making use of the weighted histogram analysis method (WHAM),[36] applied on the last 10 ns of each umbrella simulation. Umbrella sampling has been employed to determine the best surface model in term of pAntp−surface free energy of binding and thus adsorption stability.

Finally, three 100 ns long MD simulations were carried out on identified "best" (in terms of surface−pAntp interaction energy) surfaces to deeply investigate conformational and energetic properties of residues mainly involved in the pAntp−surface adsorption. Three independent system replicas (in terms of peptide−surface orientation) for each identified pAntp−surface system were generated by randomly orienting the peptide at a distance of about 1 nm to the selected surface. On each of the six generated replicas energy minimization, position restrained dynamics and production dynamics (100 ns) were carried out. The last 50 ns of each replica were taken together as data ensemble to be used for statistical analysis. GROMACS 4.6 package has been used for all MD simulations and data analysis.[37] Other adopted simulation parameters, force fields and tools employed for data analysis are reported in the Supporting Information (Figures SI.1 and SI.2).

RESULTS

Free Energy Profile of PAntp−Surface Interaction. The umbrella sampling procedure was employed to investigate the free energy landscape of SIO_2−pAntp and $hSIO_2$−pAntp interaction.[29] The energy profiles, shown in Figure 2, were reported as a function of pAntp−surface distance. Average values and standard deviation calculated by bootstrap analysis are reported. The energy well (ΔG = −18 kJ/mol) is located at a distance value of about 1 nm for SIO_2-pAntp (black curve, Figure 2a), whereas the $hSIO_2$−pAntp free energy profile (red curve, Figure 2a) is characterized by a deeper energy well (ΔG = −50 kJ/mol) located at 0.6 nm. Thus, the pAntp−surface distance at the energy minimum, as well as the free energy

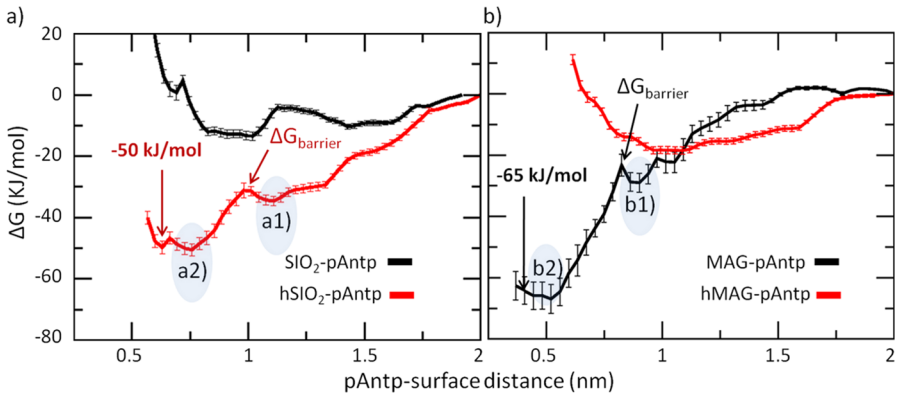

Figure 2. (a) Free energy profiles of pAntp−silica system; positions a1 and a2 on the red curve indicate minima for the pAntp−$hSiO_2$ free energy profile. (b) Free energy profiles of pAntp−magnetite system; positions b1 and b2 on the black curve indicate minima for the pAntp−$hSiO_2$ free energy profile. Error bars were estimated by standard bootstrap analysis.

DOI: 10.1021/jp512782e
J. Phys. Chem. B 2015, 119, 8239−8246

difference, seems to be strongly influenced by the surface hydroxylation state. In detail, enhanced binding affinity has been observed in the presence of hydroxylated silica surface. In the SIO_2−pAntp interaction, no remarkable energy barriers are detected (black curve, Figure 2a), while the $hSIO_2$−pAntp free energy profile is characterized by a low energy barrier (10 kJ/mol), located at 1 nm (red curve, Figure 2a). This behavior is consequence of the different peptide−surface orientation (Figure 3). In particular, the energy landscape is divided in

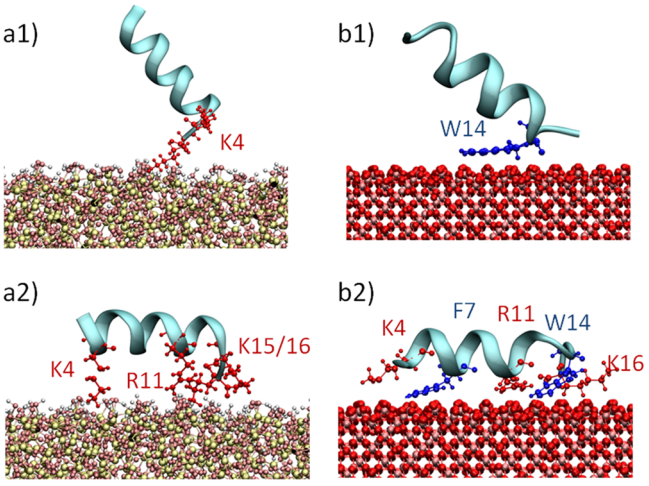

Figure 3. Visual inspection of the pAntp interaction with hSIO (a1, a2) and MAG (b1, b2) surface. The interacting residues are highlighted in red (charged residues) and blue (polar residues).

two energetically most favorable regions: when entering the first one (position a1 red curve Figure 2a), the peptide is in a standing position (snapshot a1 Figure 3), characterized by the helical axis perpendicular to the $hSIO_2$ surface. To overcome the energy barrier, the pAntp changes the helical axis orientation from perpendicular (snapshot a1 in Figure 3) to parallel (snapshot a2 in Figure 3) with respect to the surface.

Figure 2b shows the free energy profiles for pAntp−MAG (black curve, Figure 2b) and pAntp−hMAG (red curve, Figure 2b) adsorption as a function of pAntp−surface distance. By analyzing the energy landscape of pAntp−hMAG (red curve, Figure 2b) system, an energy well (−18 kJ/mol) at a pAntp−hMAG distance around 1 nm is detected. The pAntp−MAG adsorption is characterized by a deeper energy well (ΔG = −65 kJ/mol) located at of 0.5 nm (black curve, Figure 2b). The surface hydroxylation state, as previously reported for peptide adsorption on silica, strongly influences the free energy difference as well as the pAntp−surface distance corresponding to the energy minimum. Again, while no remarkable energy barriers were detected analyzing the pAntp−hMAG adsorption (red curve, Figure 2b), an energy barrier (8 kJ/mol) is detected at a distance of 0.9 nm for the pAntp−MAG system (black curve, Figure 2b). Also in this case, the adsorption is characterized by a change in orientation of the peptide helical axis (from position b1 to position b2 black curve, Figure 2b; snapshots b1 and b2, Figure 3). In detail, at the energy minimum (position b2 black curve, Figure 2b), the peptide spreads on the surface maximizing the contact surface (snapshot b2, Figure 3).

The free energy profiles reported in Figure 2 show that $hSIO_2$ and MAG are characterized by the deepest energy wells and thus the best adsorption affinity for pAntp.

Peptide−Surface Adsorption Mechanism. Three different replicas of the pAntp−$hSIO_2$ and pAntp−MAG system were simulated for 100 ns. The peptide was randomly oriented at the beginning of each simulation, with an initial separation from the surface slab of 1 nm. From these simulations we expected to obtain (i) information on the pAntp conformational changes while being adsorbed on the surface and (ii) pAntp residues involved in the adsorption mechanism.

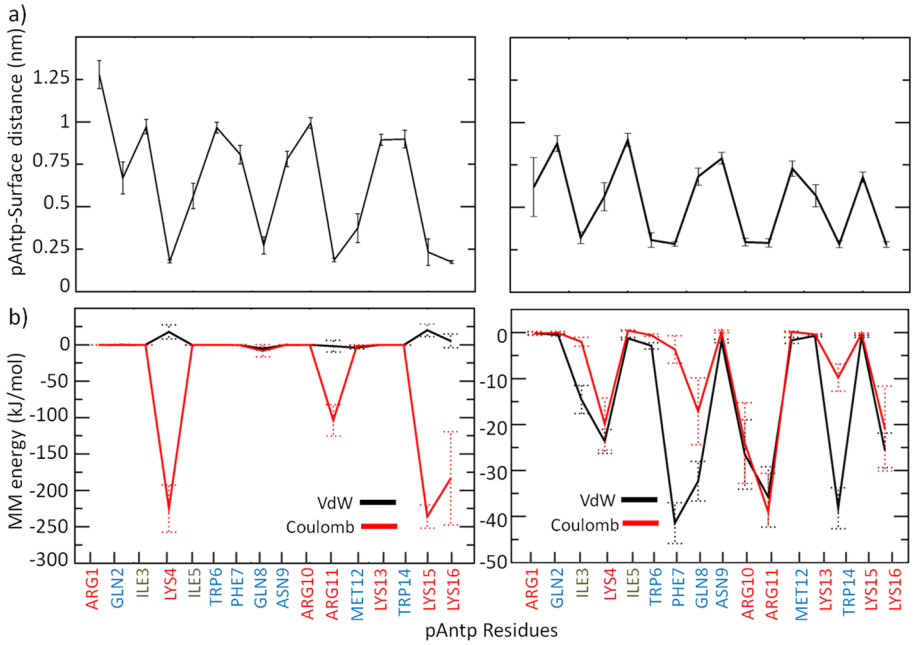

Figure 4. (a) Equilibrium distance between each pAntp residue and the interacting surface (hSIO left and MAG right, respectively). (b) Molecular mechanics energy decomposition among pAntp residues for pAntp−hSIO (left) and pAntp−MAG (right) systems. The charged residues are highlighted in red, the polar residues are highlighted in blue, and the hydrophobic residues are highlighted in green.

DOI: 10.1021/jp512782e
J. Phys. Chem. B 2015, 119, 8239−8246

In the case of pAntp−$hSIO_2$ (Figure 4), residues mainly driving the peptide−surface interaction are Lys4 (0.23 nm), Arg11 (0.25 nm), Gln8 (0.25 nm), Lys15 (0.24 nm), and Lys16 (0.23 nm). Despite the proximity to the $hSIO_2$ surface, Gln8 did not show relevant contribution to the calculated MM interaction energy. Hence, the Gln8 proximity to the surface might be driven by the tendency of the peptide to maintain an α helix conformation.

The peptide secondary structure results highly conserved during the adsorption mechanism (Supporting Information Figure SI.3). The angle of the axis of inertia of the peptide relative to the normal of the surface is $\mu = 88° \pm$ std = 4°. A decrease in the peptide diffusion constant is noticed when the peptide is adsorbed on the surface. This result is quantified in 2 orders of magnitude, indicating that the peptide mobility is limited when in contact with the surface (Supporting Information Figure SI.4).

It is interesting to get insights into the nature of the peptide−surface interaction, that is strongly driven by the electrostatic contribution (Figure 4). Results reported in Figure 4, shown in terms of molecular mechanics (MM) energy decomposition among pAntp residues, demonstrate that Lys4, Arg11, Lys15, and Lys16, all charged amino acids, are massively involved in the electrostatic noncovalent peptide−surface interactions. Electrostatic interactions between the peptide and the $hSIO_2$ mitigate the observed van der Waals repulsion, leading to adsorption of the surface.

In case of pAntp−MAG adsorption, the scenario is partially different (Figure 4): in addition to the charged residues Arg10, Arg11, and Lys16 also polar residues such as Trp6, Phe7, and Trp14 are directly involved in the peptide−surface contact area at a distance of about 0.26 nm.

Analyzing the equilibrium trajectory, we observed the peptide secondary structure highly conserved during the adsorption mechanism (Supporting Information Figure SI.3). The angle of the axis of inertia of the peptide relative to the normal of the surface is $\mu = 84°$, std = 5°.

Also in this case a decrease in the peptide diffusion constant is noticed when the peptide is adsorbed on the surface. This result is quantified in 2 orders of magnitude, indicating that the peptide mobility is limited when in contact with the surface (Supporting Information Figure SI.4).

The MM energy decomposition revealed the synergistic effect of van der Waals (VdW) attraction and electrostatic contribution to the adsorption mechanism (Figure 4). In particular, Ile4, Phe7, Arg11, Trp14, and Lys 16 are responsible for the peptide−MAG noncovalent interactions. Therefore, we find that charged residues (arginine and lysine) play a key role in binding the surface on both $hSIO_2$ and MAG. However, the peptide−MAG interaction is also driven by the VdW attraction between the surface and the polar residues Phe7 and Trp14.

DISCUSSION

Magnetic iron oxide nanoparticles have been actively investigated for their possible applications in medicine as they have represented the next generation of targeted drug delivery for more than 30 years.[14−17,38,39] Several types of iron oxide-based NPs have been developed: FeO würstite, Fe_3O_4 magnetite, α-Fe_2O_3 hematite, α-Fe_2O_3 hematite, γ-Fe_2O_3 maghemite, etc. Magnetite is the most promising and popular candidate in the field of biotechnology and drug delivery systems since it has already shown excellent biocompatibility properties.[12,13] However, as found for all nanoparticles, MNPs are characterized by a large surface-to-volume ratio, which from one side allows a very efficient functionalization, but from the other side is responsible for high surface energies and the tendency to aggregate. Moreover, the naked MAG NPs have high chemical activity, and they are easily oxidized in air, generally resulting in loss of magnetism and dispersibility. To implement the broad range of MNPs practical applications, it is extremely important to provide proper surface coating in order to control size, high magnetic properties, shape, colloidal stability, and biocompatibility. A number of computational studies are focused on the effect of different NP physicochemical properties and coatings strategies on their interaction with membranes and other.[40−50] Atomistic MD simulations have proven to be effective in describing the noncovalent interactions between NPs and biomolecules,[21] also offering a great opportunity to improve the NPs biofunctionalization, in terms of stability and affinity. Classical molecular dynamics simulation in all-atomic resolution was successfully employed in combination with experiments for the investigation of peptides adsorption mechanism on NPs to provide detailed information about the binding mechanism and the influence of point mutation on binding.[51]

Because of the pressing need to achieve these structural features, the surface of MNPs can be modified by using biomolecules such as cell penetrating peptides or coating with an inorganic layer, such as silica, ions, other metals, etc.[17] The choice of CPPs as MNPs biofunctionalization strategy represents a major breakthrough since CPPs can deliver large-cargo molecules, simultaneously being able to penetrate the cell membrane without causing significant damage.[52,53] For these reasons, detailed physical mechanisms that underlie and determine the CPPs−MAG and CPPs−silica interaction need to be clarified. In this context, computational approaches have been proven to provide the right means of obtaining the required insights, allowing the investigation of protein dynamics and protein−surfaces interaction with atomic resolution.[54−58] In this work, we have presented an atomistic investigation on the adsorption of the *Antennapedia* homeodomain-derived penetrating peptide on silica and magnetite surfaces. We provided a quantitative estimation of the pAntp−surface binding free energy by means of the umbrella sampling approach. The influence of surface hydroxylation state on the adsorption behavior was also investigated. In this work we have used two different surface models for both magnetite and silica: fully hydroxylated and completely nonhydroxylated. It is worth mentioning that the employed surface models do not have an excess of negative charge, and this likely results in an underplayed long-range electrostatics contribution to the adsorption (e.g., peptide−surface distance higher than 1.5 nm). Nevertheless, our investigation is mainly focused on the local interaction behavior, i.e., in the proximity of the surface. In this connection, the surface charge distribution of our models does depend on the defined protonation state. Hence, locally the hydroxylation state is also responsible for a different charge density over the surface. Keeping into consideration the above-mentioned limitations, the free energy results presented in this work should be better interpreted as comparative data among the considered cases more than in terms of absolute values. In summary, the main scope of this work is to provide comparative information about the effect of surface physicochemical properties on peptide adsorption.

The best surface models, in term of pAntp−surface affinity are the $hSIO_2$ and MAG surface, with an estimated adsorption

DOI: 10.1021/jp512782e
J. Phys. Chem. B 2015, 119, 8239−8246

free energy of −50 and −65 kJ/mol (Figure 2), respectively. Our results confirm that particular attention must be paid to the surface protonation state during the functionalization procedure, since the adsorption stability is strongly influenced by the exposed hydroxyl groups. Interestingly, the hydroxyl groups have a visible impact on reducing the adsorption free energy on MAG, while in the pAntp−SIO_2 system an opposite behavior was observed (Figure 2). This is consistent with the surface properties of amorphous silica demonstrated by Zhuravlev.[23] The silanol groups act as the centers of molecular adsorption and are able to form hydrogen bonds or, more generally, undergo donor−acceptor interactions. The removal of the hydroxyl groups from the surface of silica leads to an increase of the hydrophobic properties, decreasing the molecular adsorption,[23] as confirmed also in this work.

Furthermore, we have focused our effort on trying to explain a possible origin of the high peptide−surfaces affinity. We have examined the nature of this interaction, investigating how each residue of pAntp contributed to the adsorption (Figure 4). We think that our results might help in clarifying the molecular phenomena related to peptide−surface interaction by suggesting which amino acids play a major role in governing the noncovalent peptide−surface binding. The molecular mechanics energy decomposition, reported in Figure 4, has demonstrated that Lys4, Arg11, Lys15, and Lys16, all charged residues, are massively involved in the electrostatic noncovalent peptide−SIO_2 interactions. Moreover, electrostatic interactions between the peptide and the $hSIO_2$ effectively counteract the observed van der Waals repulsion, leading to strong adsorption of the surface. In the case of pAntp−MAG adsorption, synergistic effect of van der Waals (VdW) attraction and electrostatic contribution to the adsorption mechanism was observed (Figure 4). In particular, Ile4, Phe7, Arg11, Trp14, and Lys 16 are identified as mainly responsible for driving the peptide−MAG noncovalent interactions. The fact that charged residues are important players in the adsorption mechanism is not a surprising evidence per se, since the pAntp is a positively charged peptide (containing 3 Arg and 4 Lys). On the other hand, it is interesting to notice that arginine and lysine play a key role in binding both $hSIO_2$ and MAG surfaces, despite their different physicochemical properties and surface charge density.

It is worth noticing that our results are consistent with a recent computational study focused on TAT peptide,[21] which has already highlighted the role of arginine and lysine in driving peptide adsorption on silica surface. Arginine residues have been frequently found to be involved in approaching and binding hydrophobic/hydrophilic surfaces and other proteins.[54,59,60] This is probably due to their amphiphilic side chain, given that their guanidinium end groups are positively charged, whereas the aliphatic chains are hydrophobic. Computational and experimental findings have already demonstrated that arginine and lysine residues play a pivotal role in the cell membrane penetration.[1,10,61] As proposed by Kubiak-Ossowska and colleagues in the case of TAT−silica adsorption mechanism,[21] the pAntp interaction with MAG and SIO_2 hinders the availability of arginine and lysine for further membrane interactions (Figure 4). Further work is needed to engineer CPP's functionalization in a way that arginine and lysine residues are kept far away from the surface, thus being free to be used for interaction with the cell membrane.

Experimental findings[1,6] have also demonstrated that the membrane penetration of pAntp requires two different events. While in a first step, the peptide, driven by arginine and lysine residues, interacts with and enters the membrane bilayer, a second step should involve membrane destabilization where Trp6 residue seems to play a key role, necessary for full membrane traslocation.[6]

Our work suggests that pAntp−MAG interaction hampers the availability of Trp6, adsorbed on the MAG surface (Figure 4). Since this feature would impair the transient membrane destabilization, it might be possible to use selected MAG nanoparticles functionalized with pAntp, without impacting on the membrane stability. In this case it is expected that pAntp functionalized MNP would only interact, i.e. adhere, to the targeted biological membranes, remaining outside the cell.

■ ASSOCIATED CONTENT

Supporting Information

Figures SI.1−SI.7. The Supporting Information is available free of charge on the ACS Publications website at DOI: 10.1021/jp512782e.

■ AUTHOR INFORMATION

Corresponding Authors

*E-mail andrea.danani@supsi.ch (A.D.).
*E-mail antonia.follenzi@med.unipmn.it (A.F.).

Notes

The authors declare no competing financial interest.

■ REFERENCES

(1) Madani, F.; Lindberg, S.; Langel, U.; Futaki, S.; Gräslund, A. Mechanisms of Cellular Uptake of Cell-Penetrating Peptides. *J. Biophys.* **2011**, *2011*, 414729.

(2) Green, M.; Loewenstein, P. M. Autonomous Functional Domains of Chemically Synthesized Human Immunodeficiency Virus Tat Trans-Activator Protein. *Cell* **1988**, *55*, 1179−1188.

(3) Vives, E.; Brodin, P.; Lebleu, B. A Truncated HIV-1 Tat Protein Basic Domain Rapidly Translocates through the Plasma Membrane and Accumulates in the Cell Nucleus. *J. Biol. Chem.* **1997**, *272*, 16010−16017.

(4) Joliot, A.; Pernelle, C.; Deagostini-Bazin, H.; Prochiantz, A. Antennapedia Homeobox Peptide Regulates Neural Morphogenesis. *Proc. Natl. Acad. Sci. U. S. A.* **1991**, *88*, 1864−1868.

(5) Derossi, D.; Calvet, S.; Trembleau, A. Cell Internalization of the Third Helix of the Antennapedia Homeodomain Is Receptor-Independent. *J. Biol. Chem.* **1996**, *271*, 18188−18193.

(6) Dom, G. Cellular Uptake of Antennapedia Penetratin Peptides Is a Two-Step Process in Which Phase Transfer Precedes a Tryptophan-Dependent Translocation. *Nucleic Acids Res.* **2003**, *31*, 556−561.

(7) Maniti, O.; Blanchard, E.; Trugnan, G.; Lamazière, A.; Ayala-Sanmartin, J. Metabolic Energy-Independent Mechanism of Internalization for the Cell Penetrating Peptide Penetratin. *Int. J. Biochem. Cell Biol.* **2012**, *44*, 869−875.

(8) Alves, I.; Bechara, C.; Walrant, A.; Zaltsman, Y. Relationships between Membrane Binding, Affinity and Cell Internalization Efficacy of a Cell-Penetrating Peptide: Penetratin as a Case Study. *PLoS One* **2011**, *6*.

(9) Derossi, D.; Joliot, A. The Third Helix of the Antennapedia Homeodomain Translocates through Biological Membranes. *J. Biol. Chem.* **1994**, *269*, 10444−10450.

(10) Pourmousa, M.; Karttunen, M. Early Stages of Interactions of Cell-Penetrating Peptide Penetratin with a DPPC Bilayer. *Chem. Phys. Lipids* **2013**, *169*, 85−94.

(11) Bele, M.; Hribar, G.; Čampelj, S.; Makovec, D.; Gaberc-Porekar, V.; Zorko, M.; Gaberšček, M.; Jamnik, J.; Venturini, P. Zinc-Decorated Silica-Coated Magnetic Nanoparticles for Protein Binding and Controlled Release. *J. Chromatogr. B: Anal. Technol. Biomed. Life Sci.* **2008**, *867*, 160−164.

DOI: 10.1021/jp512782e
J. Phys. Chem. B 2015, 119, 8239−8246

(12) Yen, S. K.; Padmanabhan, P.; Selvan, S. T. Multifunctional Iron Oxide Nanoparticles for Diagnostics, Therapy and Macromolecule Delivery. *Theranostics* **2013**, *3*, 986−1003.
(13) Laurent, S.; Saei, A. A.; Behzadi, S.; Panahifar, A.; Mahmoudi, M. Superparamagnetic Iron Oxide Nanoparticles for Delivery of Therapeutic Agents: Opportunities and Challenges. *Expert Opin. Drug Delivery* **2014**, *11*, 1−22.
(14) Hofmann, A.; Wenzel, D.; Becher, U. M.; Freitag, D. F.; Klein, A. M.; Eberbeck, D.; Schulte, M.; Zimmermann, K.; Bergemann, C.; Gleich, B.; et al. Combined Targeting of Lentiviral Vectors and Positioning of Transduced Cells by Magnetic Nanoparticles. *Proc. Natl. Acad. Sci. U. S. A.* **2009**, *106*, 44−49.
(15) Wenzel, D.; Rieck, S.; Vosen, S.; Mykhaylyk, O.; Trueck, C.; Eberbeck, D.; Trahms, L.; Zimmermann, K.; Pfeifer, A.; Fleischmann, B. K. Identification of Magnetic Nanoparticles for Combined Positioning and Lentiviral Transduction of Endothelial Cells. *Pharm. Res.* **2012**, *29*, 1242−1254.
(16) Trueck, C.; Zimmermann, K.; Mykhaylyk, O.; Anton, M.; Vosen, S.; Wenzel, D.; Fleischmann, B. K.; Pfeifer, A. Optimization of Magnetic Nanoparticle-Assisted Lentiviral Gene Transfer. *Pharm. Res.* **2012**, *29*, 1255−1269.
(17) Wu, W.; He, Q.; Jiang, C. Magnetic Iron Oxide Nanoparticles: Synthesis and Surface Functionalization Strategies. *Nanoscale Res. Lett.* **2008**, *3*, 397−415.
(18) Pietronave, S.; Iafisco, M.; Locarno, D.; Rimondini, L.; Maria Prat, M. Functionalized Nanomaterials for Diagnosis and Therapy of Cancer. *J. Appl. Biomater. Biomech.* **2009**, *7*, 77−89.
(19) Schladt, T. D.; Schneider, K.; Schild, H.; Tremel, W. Synthesis and Bio-Functionalization of Magnetic Nanoparticles for Medical Diagnosis and Treatment. *Dalton Trans.* **2011**, *40*, 6315−6343.
(20) Turcheniuk, K.; Tarasevych, A. V.; Kukhar, V. P.; Boukherroub, R.; Szunerits, S. Recent Advances in Surface Chemistry Strategies for the Fabrication of Functional Iron Oxide Based Magnetic Nanoparticles. *Nanoscale* **2013**, *5*, 10729−10752.
(21) Kubiak-Ossowska, K.; Burley, G.; Patwardhan, S. V.; Mulheran, P. A. Spontaneous Membrane-Translocating Peptide Adsorption at Silica Surfaces: A Molecular Dynamics Study. *J. Phys. Chem. B* **2013**, *117*, 14666−14675.
(22) Humphrey, W.; Dalke, A.; Schulten, K. VMD: Visual Molecular Dynamics. *J. Mol. Graphics* **1996**, *14*, 33−38 27−28..
(23) Zhuravlev, L. T. The Surface Chemistry of Amorphous Silica. Zhuravlev Model. *Colloids Surf., A* **2000**, *173*, 1−38.
(24) Leroch, S.; Wendland, M. Simulation of Forces between Humid Amorphous Silica Surfaces: A Comparison of Empirical Atomistic Force Fields. *J. Phys. Chem. C* **2012**, *116*, 26247−26261.
(25) Cygan, R. T.; Liang, J.-J.; Kalinichev, A. G. Molecular Models of Hydroxide, Oxyhydroxide, and Clay Phases and the Development of a General Force Field. *J. Phys. Chem. B* **2004**, *108*, 1255−1266.
(26) Skelton, A. A.; Wesolowski, D. J.; Cummings, P. T. Investigating the Quartz (1010)/Water Interface Using Classical and Ab Initio Molecular Dynamics. *Langmuir* **2011**, *27*, 8700−8709.
(27) Skelton, A. A.; Fenter, P.; Kubicki, J. D.; Wesolowski, D. J.; Cummings, P. T. Simulations of the Quartz$(10\bar{1}1)$/Water Interface: A Comparison of Classical Force Fields, Ab Initio Molecular Dynamics, and X-Ray Reflectivity Experiments. *J. Phys. Chem. C* **2011**, *115*, 2076−2088.
(28) Gale, J. D.; Rohl, A. L. The General Utility Lattice Program (GULP). *Mol. Simul.* **2003**, *29*, 291−341.
(29) Rappé, A. K.; Goddard, W. A., III Charge Equilibration for Molecular Dynamics Simulations. *J. Phys. Chem.* **1991**, *95*, 3358−3363.
(30) Lindberg, M.; Biverståhl, H.; Gräslund, A.; Mäler, L. Structure and Positioning Comparison of Two Variants of Penetratin in Two Different Membrane Mimicking Systems by NMR. *Eur. J. Biochem.* **2003**, *270*, 3055−3063.
(31) Mackerell, A. D.; Feig, M.; Brooks, C. L. Extending the Treatment of Backbone Energetics in Protein Force Fields: Limitations of Gas-Phase Quantum Mechanics in Reproducing Protein Conformational Distributions in Molecular Dynamics Simulation. *J. Comput. Chem.* **2004**, *25*, 1400−1415.
(32) MacKerell, a D.; Bashford, D.; Bellott, M.; Dunbrack, R. L.; Evanseck, J. D.; Field, M. J.; Fischer, S.; Gao, J.; Guo, H.; Ha, S.; et al. All-Atom Empirical Potential for Molecular Modeling and Dynamics Studies of Proteins. *J. Phys. Chem. B* **1998**, *102*, 3586−3616.
(33) Heine, D. R.; Rammohan, A. R.; Balakrishnan, J. Atomistic Simulations of the Interaction between Lipid Bilayers and Substrates. *Mol. Simul.* **2007**, *33*, 391−397.
(34) Payne, C. M.; Zhao, X.; Vlcek, L.; Cummings, P. T. Molecular Dynamics Simulation of Ss-DNA Translocation between Copper Nanoelectrodes Incorporating Electrode Charge Dynamics. *J. Phys. Chem. B* **2008**, *112*, 1712−1717.
(35) Ricci, M.; Spijker, P.; Voïtchovsky, K. Water-Induced Correlation between Single Ions Imaged at the Solid-Liquid Interface. *Nat. Commun.* **2014**, *5*, 4400.
(36) Kumar, S.; Rosenberg, J. M.; Bouzida, D.; Swendsen, R. H.; Kollman, P. A. THE Weighted Histogram Analysis Method for Free-Energy Calculations on Biomolecules. I. The Method. *J. Comput. Chem.* **1992**, *13*, 1011−1021.
(37) Hess, B.; Kutzner, C.; van der Spoel, D.; Lindahl, E. GROMACS 4: Algorithms for Highly Efficient, Load-Balanced, and Scalable Molecular Simulation. *J. Chem. Theory Comput.* **2008**, *4*, 435−447.
(38) Frimpong, R. A.; Hilt, J. Z. Magnetic Nanoparticles in Biomedicine: Synthesis, Functionalization and Applications. *Nanomedicine* **2010**, *5*, 1401−1414.
(39) Veiseh, O.; Gunn, J. W.; Zhang, M. Design and Fabrication of Magnetic Nanoparticles for Targeted Drug Delivery and Imaging. *Adv. Drug Delivery Rev.* **2010**, *62*, 284−304.
(40) Gkeka, P.; Angelikopoulos, P.; Sarkisov, L.; Cournia, Z. Membrane Partitioning of Anionic, Ligand-Coated Nanoparticles Is Accompanied by Ligand Snorkeling, Local Disordering, and Cholesterol Depletion. *PLoS Comput. Biol.* **2014**, *10*, e1003917.
(41) Prates Ramalho, J. P.; Gkeka, P.; Sarkisov, L. Structure and Phase Transformations of DPPC Lipid Bilayers in the Presence of Nanoparticles: Insights from Coarse-Grained Molecular Dynamics Simulations. *Langmuir* **2011**, *27*, 3723−3730.
(42) Gkeka, P.; Angelikopoulos, P. The Role of Patterned Hydrophilic Domains in Nanoparticle-Membrane Interactions. *Curr. Nanosci.* **2011**, *7*, 690−698.
(43) Jusufi, A.; DeVane, R. H.; Shinoda, W.; Klein, M. L. Nanoscale Carbon Particles and the Stability of Lipid Bilayers. *Soft Matter* **2011**, *7*, 1139.
(44) Udayana Ranatunga, R. J. K.; Kalescky, R. J. B.; Chiu, C. C.; Nielsen, S. O. Molecular Dynamics Simulations of Surfactant Functionalized Nanoparticles in the Vicinity of an Oil/Water Interface. *J. Phys. Chem. C* **2010**, *114*, 12151−12157.
(45) Lin, X.; Li, Y.; Gu, N. Nanoparticle's Size Effect on Its Translocation across a Lipid Bilayer: A Molecular Dynamics Simulation. *J. Comput. Theor. Nanosci.* **2010**, *7*, 269−276.
(46) Gkeka, P.; Sarkisov, L.; Angelikopoulos, P. Homogeneous Hydrophobic-Hydrophilic Surface Patterns Enhance Permeation of Nanoparticles through Lipid Membranes. *J. Phys. Chem. Lett.* **2013**, *4*, 1907−1912.
(47) Langel, U. *Handbook of Cell-Penetrating Peptides*, 2nd ed.; CRC Press Taylor & Francis Group: Boca Raton, FL, 2006; Vol. *40*.
(48) Lättig-Tünnemann, G.; Prinz, M.; Hoffmann, D.; Behlke, J.; Palm-Apergi, C.; Morano, I.; Herce, H. D.; Cardoso, M. C. Backbone Rigidity and Static Presentation of Guanidinium Groups Increases Cellular Uptake of Arginine-Rich Cell-Penetrating Peptides. *Nat. Commun.* **2011**, *2*, 453.
(49) Gkeka, P.; Sarkisov, L. Interactions of Phospholipid Bilayers with Several Classes of Amphiphilic a-Helical Peptides: Insights from Coarse-Grained Molecular Dynamics Simulations. *J. Phys. Chem. B* **2010**, *114*, 826−839.
(50) Yesylevskyy, S.; Marrink, S. J.; Mark, A. E. Alternative Mechanisms for the Interaction of the Cell-Penetrating Peptides Penetratin and the TAT Peptide with Lipid Bilayers. *Biophys. J.* **2009**, *97*, 40−49.
(51) Patwardhan, S. V.; Emami, F. S.; Berry, R. J.; Jones, S. E.; Naik, R. R.; Deschaume, O.; Heinz, H.; Perry, C. C. Chemistry of Aqueous

DOI: 10.1021/jp512782e
J. Phys. Chem. B 2015, 119, 8239−8246

Silica Nanoparticle Surfaces and the Mechanism of Selective Peptide Adsorption. *J. Am. Chem. Soc.* **2012**, *134*, 6244−6256.
(52) Sanders, W. S.; Johnston, C. I.; Bridges, S. M.; Burgess, S. C.; Willeford, K. O. Prediction of Cell Penetrating Peptides by Support Vector Machines. *PLoS Comput. Biol.* **2011**, *7*, e1002101.
(53) Thomas, A.; Lins, L.; Divita, G.; Brasseur, R. Realistic Modeling Approaches of Structure-Function Properties of CPPs in Non-Covalent Complexes. *Biochim. Biophys. Acta* **2010**, *1798*, 2217−2222.
(54) Apicella, A.; Soncini, M.; Deriu, M. A.; Natalello, A.; Bonanomi, M.; Dellasega, D.; Tortora, P.; Regonesi, M. E.; Casari, C. S. A Hydrophobic Gold Surface Triggers Misfolding and Aggregation of the Amyloidogenic Josephin Domain in Monomeric Form, While Leaving the Oligomers Unaffected. *PLoS One* **2013**, *8*, e58794.
(55) Deriu, M. A.; Enemark, S.; Soncini, M.; Montevecchi, F. M.; Redaelli, A. Tubulin: From Atomistic Structure to Supramolecular Mechanical Properties. *J. Mater. Sci.* **2007**, *42*, 8864−8872.
(56) Deriu, M. A.; Shkurti, A.; Paciello, G.; Bidone, T. C.; Morbiducci, U.; Ficarra, E.; Audenino, A.; Acquaviva, A. Multiscale Modeling of Cellular Actin Filaments: From Atomistic Molecular to Coarse-Grained Dynamics. *Proteins: Struct., Funct., Bioinf.* **2012**, *80*, 1598−1609.
(57) M. Pavan, G.; Monteagudo, S.; Guerra, J.; Carrion, B.; Ocana, V.; Rodriguez-Lopez, J.; Danani, A.; C. Perez-Martinez, F.; Cena, V. Role of Generation, Architecture, pH and Ionic Strength on Successful siRNA Delivery and Transfection by Hybrid PPV-PAMAM Dendrimers. *Curr. Med. Chem.* **2012**, *19*, 4929−4941.
(58) Furlan, S.; La Penna, G.; Appelhans, D.; Cangiotti, M.; Ottaviani, M. F.; Danani, A. Combined EPR and Molecular Modeling Study of PPI Dendrimers Interacting with Copper Ions: Effect of Generation and Maltose Decoration. *J. Phys. Chem. B* **2014**, *118*, 12098−12111.
(59) Deriu, M. A.; Grasso, G.; Licandro, G.; Danani, A.; Gallo, D.; Tuszynski, J. A.; Morbiducci, U. Investigation of the Josephin Domain Protein-Protein Interaction by Molecular Dynamics. *PLoS One* **2014**, *9*, e108677.
(60) Koch, R.; Lipton, A. S.; Filipek, S.; Renugopalakrishnan, V. Arginine Interactions with Anatase TiO_2 (100) Surface and the Perturbation of 49Ti NMR Chemical Shifts - A DFT Investigation: Relevance to Renu-Seeram Bio Solar Cell. *J. Mol. Model.* **2011**, *17*, 1467−1472.
(61) Kawamoto, S.; Takasu, M.; Miyakawa, T.; Morikawa, R.; Oda, T.; Futaki, S.; Nagao, H. Inverted Micelle Formation of Cell-Penetrating Peptide Studied by Coarse-Grained Simulation: Importance of Attractive Force between Cell-Penetrating Peptides and Lipid Head Group. *J. Chem. Phys.* **2011**, *134*, 095103.

DOI: 10.1021/jp512782e
J. Phys. Chem. B 2015, 119, 8239−8246